Heliyon 10 (2024) e37966

Contents lists available at ScienceDirect

Heliyon

journal homepage: www.cell.com/heliyon

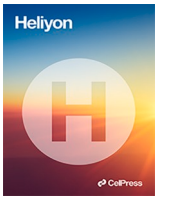

Research article

Development of biological techniques to prevent corrosion of reinforcing steel bars

Sajid Rasheed [a], Rao Arslan Khushnood [a], Ali Raza [a,c,*], Sajjad Ahmed [b], Maria Kanwal [a]

[a] NUST Institute of Civil Engineering (NICE), School of Civil and Environmental Engineering (SCEE), National University of Sciences and Technology (NUST), H/12 Campus, Islamabad, 44000, Pakistan
[b] University College of Engineering and Technology, Bahauddin Zakaria University, Multan, Pakistan
[c] School of Civil and Environmental Engineering, University of New South Wales (UNSW Sydney), Sydney, NSW, 2052, Australia

ARTICLE INFO

Keywords:
Encapsulation
Biofilm
Corrosion inhibition
Microstructure refinement
Split tensile strength

ABSTRACT

The electrochemical corrosive processes compromise the passivity of reinforcing steel, potentially leading to structural integrity loss and, in extreme cases, concrete infrastructure failures. While bio-inspired concretes show promise in mitigating strength degradation and enabling self-healing of concrete flaws, their interaction with steel reinforcement remains underexplored. Thus, this investigation aimed to establish a protective strategy by fostering biofilm growth on rebar surfaces. To achieve this, *Bacillus subtilis* and *Escherichia coli* bacteria were utilized as biofilm-forming agents, aided by magnetic iron oxide and zeolite micro-nano particles. The study encompassed a thorough assessment of split tensile strength, corrosion resistance of bio-treated embedded steel bars, and a comprehensive biofilm characterization, along with a meticulous examination of the microstructure at the steel-concrete interface. The findings underscored a significant improvement in split tensile strength, demonstrating a remarkable 84.2 % increase when bacterial species were combined with iron oxide nanoparticles, in contrast to the control specimens. Furthermore, the bio-treated bars exhibited an impressive corrosion inhibition potential of 78.5 % relative to their unaltered counterparts. These outcomes are attributed to the discernible refinement of microstructural features surrounding the steel reinforcement and the heightened densification of the inter-transitional zone between steel and concrete.

1. Introduction

Concrete, a globally prevalent and cost-effective material, boasts a wide range of versatile mechanical properties [1–3]. However, its vulnerability to flexural and tensile loading undermines its popularity. To address this, steel is incorporated into concrete as a compatible material, enhancing its resistance to both flexural and tensile stresses [4,5]. During service life, concrete undergoes various environmental influences, which lead to crack generation. These cracks provide pathways to harmful environmental ingredients like moisture, carbon dioxide, chlorides, oxygen, and ammonia to jump into the concrete microstructure [6]. This aggressive medium affects the alkalinity of concrete resulting in de-passivation of the protective layer on steel and causing corrosion [7–10].

* Corresponding author. NUST Institute of Civil Engineering (NICE), School of Civil and Environmental Engineering (SCEE), National University of Sciences and Technology (NUST), H/12 Campus, Islamabad, 44000, Pakistan.
E-mail addresses: ali.raza@unsw.edu.au, aliraza.must@gmail.com (A. Raza).

https://doi.org/10.1016/j.heliyon.2024.e37966
Received 21 February 2024; Received in revised form 13 September 2024; Accepted 14 September 2024
Available online 14 September 2024

Table 1
Chemical composition of cement.

CaO	SiO_2	Al_2O_3	Fe_2O_3	SO_3	MgO	K_2O
63.4	20.3	4.88	3.2	2.7	2.4	0.5

Table 2
Properties of aggregate [52].

Materials ID	FM	Specific gravity SSD	Specific Gravity OD	Apparent Specific Gravity	Absorption (%)
FA	2.713	2.6	2.532	2.717	2.7
CA	–	2.683	2.664	2.715	0.7

Corrosion is an electrochemical process that involves the transfer of electrons from the anode to the cathode and deposits rust on the steel surface [11]. This rust causes strength and durability loss of reinforced concrete structures [12]. 15–20 % corrosion of steel triggers brittle failure of reinforced structures and the nature of failure becomes more or less catastrophic [13,14]. Service life of structures significantly decreases due to corrosion as 20 % mass loss of steel in reinforced concrete could reduce 70 % of concrete age and 80 % of strength [15]. Each year, the United States allocates over 20 billion USD, and the United Kingdom dedicates around 600 million USD for the maintenance of highways and bridges [16]. Remarkably, this accounts for a substantial 85 % of the total project cost. Repair of corrosion structures is not possible leads to the demolition of structures [17–19]. 90 of the structures having corrosion issues were demolished in the USA due to a risk of structure failure from the steel and concrete bond zone [12]. 12 % corrosion of steel results in 70 % bond strength loss [14]. Corrosion is a more rapid phenomenon than other degradations of RC structures and a prime reason for the detrimental destruction of RC structures [15].

Demolishing concrete structures produces concrete waste and new concrete construction is not a sustainable solution due to its significant effect on climate changes [20,21]. USA demolished waste reaches 143 trillion metric tons annually which is only due to the corrosion of reinforced concrete structures and new construction of concrete structures produces huge amounts of carbon dioxide and causes global warming [22,23]. Corrosion of steel can be mitigated and prevented by chemical, physical, electrical, and biological means [24,25]. However, chemical treatments and coatings on steel bars reduce the bond strength between steel and concrete [26].

However, several bacterial strains can survive on metal surfaces and produce a biofilm that is an environment-friendly layer and preserve metal faces from environmental degradations [27]. Studies reported that *Escherichia coli (E. coli)* and *Bacillus subtilis (B. subtilis)* are good biofilm forming bacteria and the growth of bacteria on the surface of pristine metal has long-term survivability [28–30]. The performance of bacteria changes from species to species and according to the subjected environmental conditions [31–34].

The incorporation of bacteria in concrete is showing promising outcomes in terms of durability and mechanical aspects. The self-healing concrete studies show that the bacterial addition in concrete produces calcite and improves the confinement of concrete microstructure [35–37]. For instance, bacteria like *B. subtilis* precipitated calcium carbonate in concrete cracks and fishers and densified the microstructure [38–41]. Bacteria experience high alkalinity (pH $>$ 12) and stresses during the mixing of concrete therefore their survival can be compromised. Therefore, the incorporation of bacterial species with a protective carrier medium is very common and essential too which could act as a host media for the bacteria in the harsh environment of concrete [41–46]. Whereas the interaction of these bio-species with reinforcing bars is yet to be investigated.

Thus, in this study, the behavior of two biofilm-forming strains on the surface of steel bars has been explored. The surface of steel bars was biologically treated by growing biofilms of *E. coli* and *B. subtilis* and then embedded in concrete. The micro-nano-sized magnetic iron oxide particles and magnetic zeolite particles were selected as bacterial carrier medium. The corrosion inhibition and improvement in inter transition zone (ITZ) of steel and concrete along with microstructural refinement of the specimens were investigated as prime objectives of this study.

2. Materials and methods

The ASTM type 1, Ordinary Portland cement was used as binding material ASTM-C150 [47]. The composition of cement is listed in Table 1. The particle size was less than 75 μm and passed from sieve no. 200. The percentage retained weight on sieve no. 200 was less the 2 % that was within the allowable limits of ASTM C184 [48]. The initial and final setting times of cement were tested by vacate apparatus following the testing procedure of ASTM C403 [49]. It was recorded as 47 and 195 min, respectively. The cement was tested for LOI value for 15 min in the oven at 900^{o}C and percentage loss was recorded at 1 % which is within the range of ASTM C114.

Locally available Lawrancepur sand was used as fine aggregates (FA). Sieve analysis according to ASTM C33 [50] was performed to get particle size distribution and fineness modulus (FM). Water absorption was determined according to ASTM C128 [51] as given in Table 2. Locally available Marghla crush was used as coarse aggregates (CA). The particle size of CA was determined by sieve analysis according to ASTM C33. Water absorption value and specific gravity were also defined according to ASTM C127 [52] as presented in Table 2.

Grade 40 deformed #3 steel bars were procured from “ITHAAD STEEL INDUSTRIES”. The physical properties were satisfying the

Table 3
Properties of steel [53].

Nominal Diameter	Cross Section Area	Yield		Tensile Strength		Gauge Length		Elongation
		Load	Stress	Ultimate Load	Stress	Actual	Increased	Achieved
(inch)	(in^2)	(KN)	(Psi)	(KN)	(Psi)	(inch)	(inch)	(%)
3/8	0.11	26.1	53273	30.61	62560	8	1.47	18.37

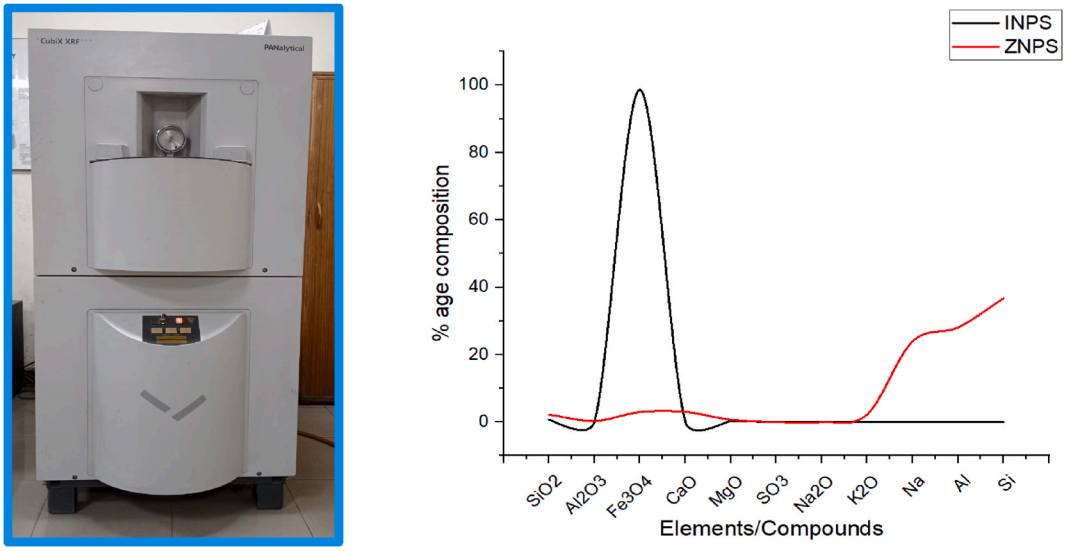

Fig. 1. X-ray fluorescence test for zeolite and iron nano-micro particles.

Table 4
Composition of zeolite and iron nano-micro particles.

Compounds /Oxides	SiO_2	Al_2O_3	Fe_3O_4	CaO	MgO	K_2O
INMPs	0.7	0.15	98.6	0.157	0.26	0.12
ZNMPs	46.8	33.96	4.95	4.2	0.75	3.21

ASTM-A615M [53]. A tensile strength test was performed on the rebars, the results of the test are listed in Table 3.

Iron-oxide nano-micro particles (INMPs) and Zeolite nano-micro particles (ZNMPs) were selected as carrier media for the study based on the literature. Nanoparticles of iron are metallic nano inclusions that impart magnetic influence. Zeolite is a crystalline hydrated solid and chemically contains aluminum and silicates. The chemical composition of both carrier media was investigated by PANalytical B.V. CubiX XRF instrument shown in Fig. 1 by following ASTM E572 [54]. The results of oxide composition are given in Table 4.

Particle size distribution confirmed that the average size of particles is 0.172 μm and 0.375 μm for ZNMPs and INMPs, respectively as shown in Fig. 2. Iron oxide inspired researchers due to its magnetic properties. Nano/microparticles of iron oxide were magnetic in nature and tested for magnetic properties. The arrangement was made according to ASTM A894 [55]. The polarity of the material was investigated by the "*E29 VSM* instrument" and readings of magnetization hysteresis and remanence were obtained. For the VSM apparatus 5g of INMPs and ZNMPs sample was put into charge jar and tested for magnetic saturation. Results are shown in Table 5.

The magnetic saturation value of the materials lies in the range of magnetic materials which is highlighted by previous studies. The hysteresis saturation value also pointed out that the material is magnetic in nature.

B. subtilis is a gram-positive, non-pathogenic, and rod-shaped bacterium. It is available in the soil and human body. It is alkaliphilic in nature and possesses longtime survival. Whereas *E. coli* is a gram-negative and anaerobic bacterium that is shaped like a rod and affected by a magnetic field. These two species are selected based on the biofilm forming abilities along with compatibility with the carrier medium. It is of both pathogenic and non-pathogenic nature. Its non-pathogenic 5α is highly recommended for biotechnology. The gram staining of bacteria confirmed the gram-positive and gram-negative nature of *B. subtilis* and *E. coli*, respectively. The tube-shaped pink color membrane and rodlike shape and purple color membrane identified *e. coli* as gram-negative in Fig. 3 (a). *B. subtilis* as gram-positive in Fig. 3 (b), respectively. The behavior of gram-positive and negative bacteria is different with magnetic materials. The selection of two different types of strains was based on carrying the comparative studies of the bacterial performance and compatibility

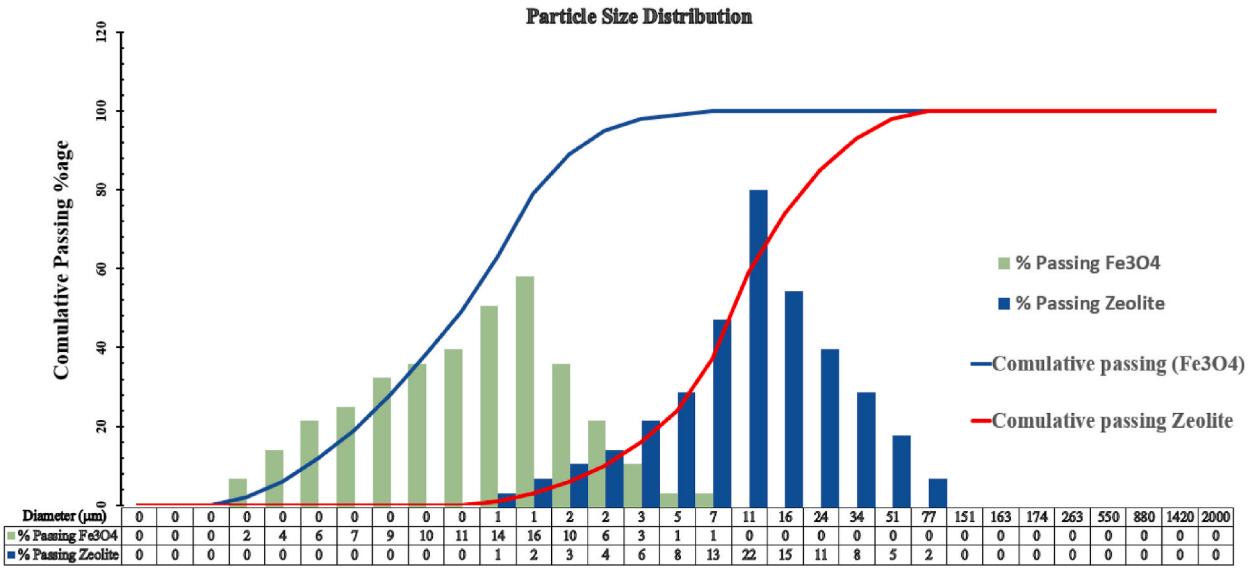

Diameter (μm)	0	0	0	0	0	0	0	0	0	0	1	1	2	2	3	5	7	11	16	24	34	51	77	151	163	174	263	550	880	1420	2000
% Passing Fe3O4	0	0	0	2	4	6	7	9	10	11	14	16	10	6	3	1	1	0	0	0	0	0	0	0	0	0	0	0	0	0	0
% Passing Zeolite	0	0	0	0	0	0	0	0	0	0	1	2	3	4	6	8	13	22	15	11	8	5	2	0	0	0	0	0	0	0	0

Fig. 2. Laser particle size analysis for zeolite and iron.

Table 5
Vibration Sample Magnetometer results for zeolite and iron.

Properties	Upward Part	Downward Part	Average
INMPs			
MS (emu)	374.57	−374.432	374.444
Hc Offset (Oe)	128.853	128.853	128.853
Hn (Oe)	5318.733	−5043.050	5180.891
Hs (Oe)	5717.221	−5545.613	5631.417
ZNMPs			
MS (emu)	123.2	−119.32	120.26
Hc Offset (Oe)	152.912	152.912	152.912
Hn (Oe)	4977.351	−4263.225	4620.288
Hs (Oe)	5210.602	−5133.823	5172.213

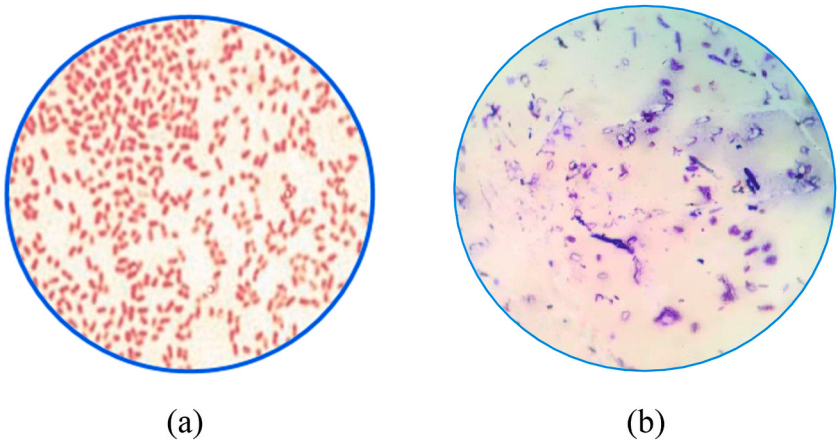

Fig. 3. Optical microscopy of (a) *Escherichia coli* (b) Bacillus subtilis.

with the magnetic carrier medium.

Bacteria were cultured on a Petri plate surface using nutrient agar as bacterial food. After successful growth on the plate bacteria is then inoculated in nutrient broth media. The optical density (OD) of bacterial strains was observed by a UV spectrophotometer of a well-homogenized solution of bacteria in distilled water. The reference medium selected for the OD was distilled water. For this

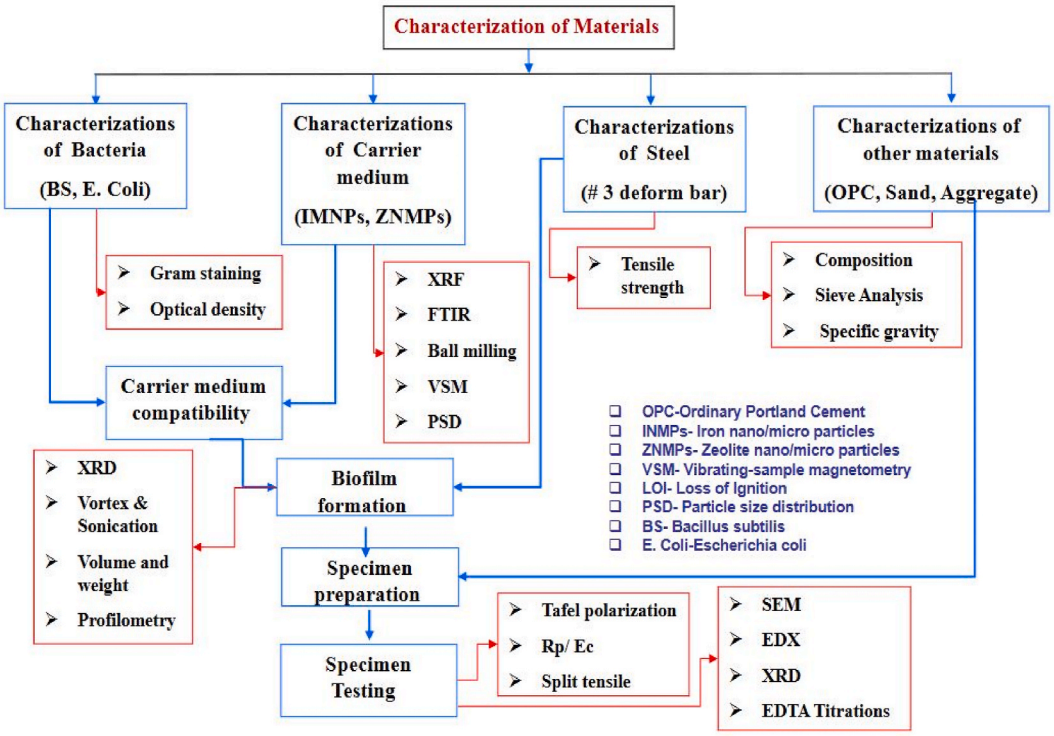

Fig. 4. Experimental flow chart.

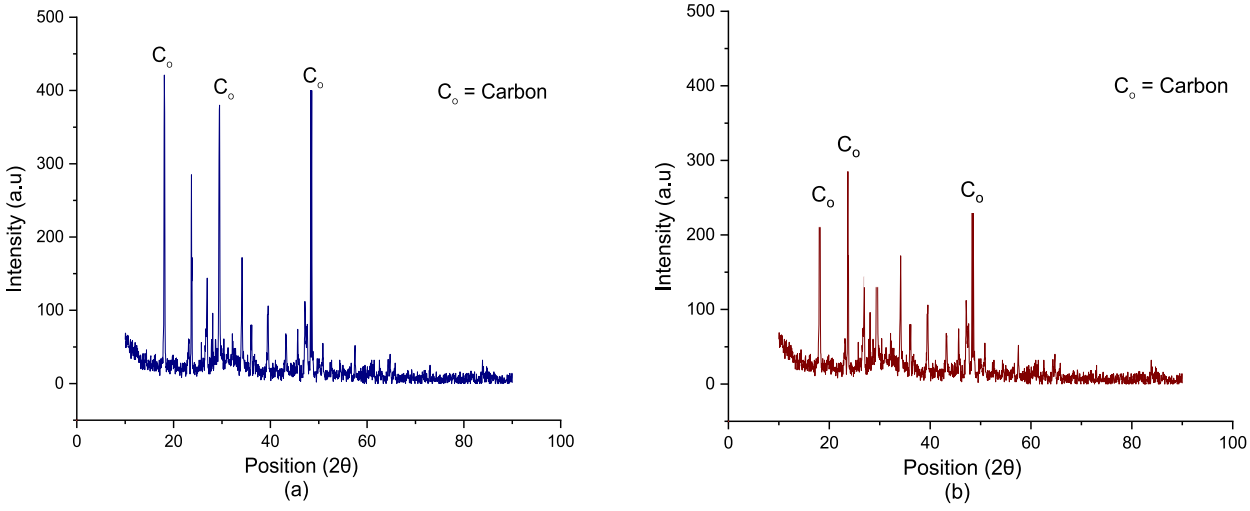

Fig. 5. XRD of biofilm (a) *Bacillus subtilis* (b) *Escherichia coli.*

purpose, the standard procedure of ASTM D1500 (ASTM d1500 | Color | Oil n.d.) was followed. Two civets, one filled with bacterial solution and one with reference solution were put in the unit after feeding the reference media values and the observed for the value of optical density. OD for bacterial strains was maintained at 0.5 to perform comparable analysis on biofilms by two distinct microbes. The compatibility of bacterial strains with INMPs and ZNMPs was tested by observing the successful growth of bacteria on petri plates containing INMPs and ZNMPs along with nutrient agar.

Calcium Lactate Penta Hydrate ($Ca(CH_2CHOHCOO)_2.5H_2O$), was used as a feeding medium for bacteria in concrete. 5 % of refined sodium chloride salt was used during corrosion testing; it was added to filtered water to prepare the electrolyte.

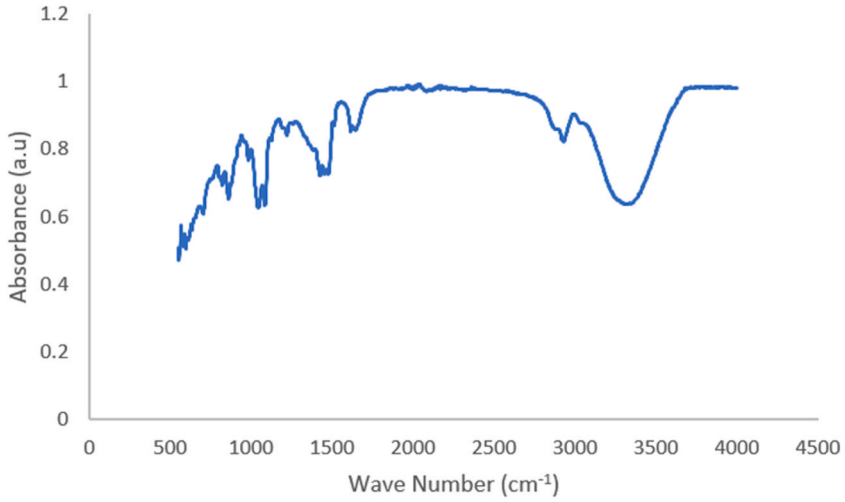

Fig. 6a. FTIR results for zeolite.

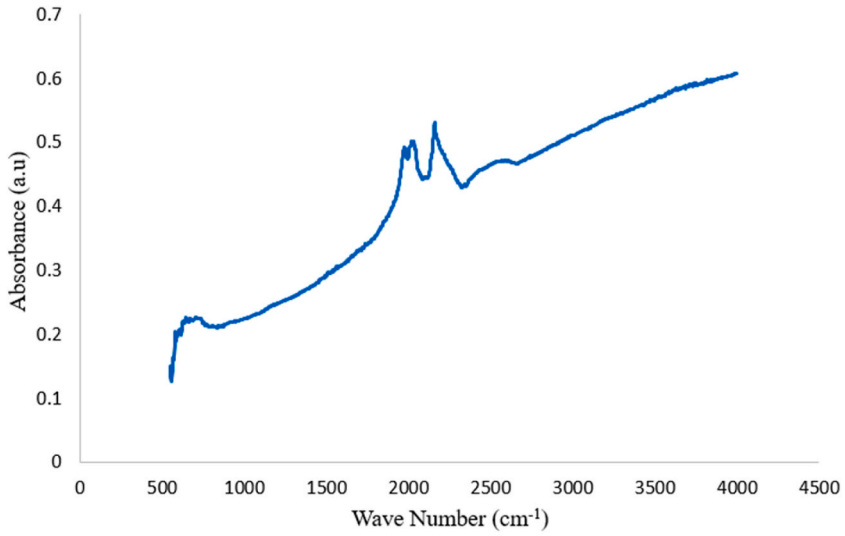

Fig. 6b. FTIR results for iron-oxide.

3. Experimental program

The experimental program along with flow of activities is shown in Fig. 4.

3.1. Bacterial biofilm

Bacterial biofilm was prepared on the surface of steel bar by placing it in a glass column filled with bacterial solution, set in a shaking incubator for 72 h at 37^{o}C and 200 rpm following the procedure reported in F. Zameer et al., 2010 studies[56–59]. Biofilm was then investigated quantitatively and qualitatively. For the quality testing biofilm was removed from the surface of the steel bar by a spatula and layers were dried at room temperature for three days and then ground into powdered form. XRD of the powder confirmed that it contained *B. subtilis* shown in Fig. 5 (a) and E E. coli shown in Fig. 5 (b). Results were comparable with Afifudin et al., 2011 [60] and K Deplanche et al., 2010 [61] respectively.

For the elemental detention of the carrier medium FTIR test was performed that confirmed the elemental purity of zeolite and iron oxide. The results of FTIR are shown below in Fig. 6 (a) and 6 (b). When carrier medium was added, FTIR analysis was performed to check deviations of the graph from the actual graph of iron-oxide and zeolite. The ALPHA I compact FT-IR spectrometer was used to carry out this test. Plots of zeolite, zeolite with *E. coli,* and zeolite with *B. subtilis* are shown in Fig. 7 (a), and iron oxide, iron oxide with *E. coli* and iron oxide with Bacillus subtilis Shown in Fig. 7 (b). Results showed that bacterial strains were successfully incorporated in

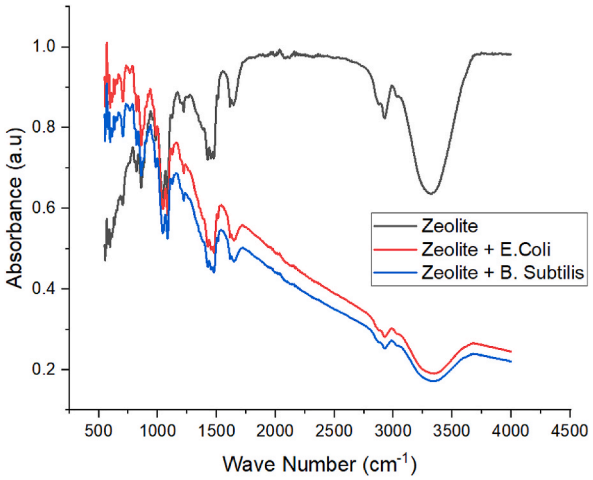

Fig. 7a. FTIR results for zeolite and bacterial additions.

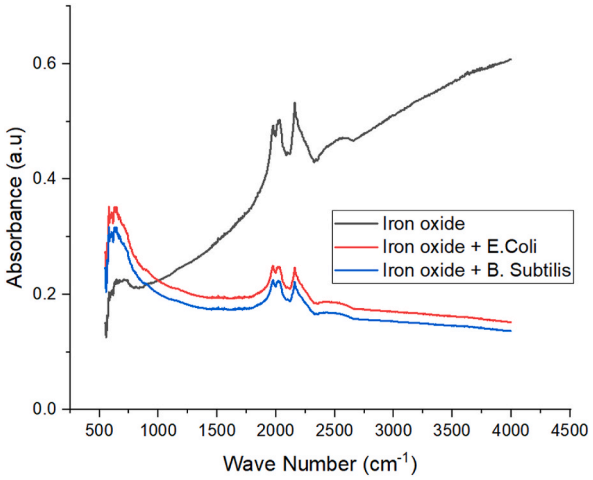

Fig. 7b. FTIR results for iron oxide and bacterial additions.

carrier media and showed new patterns on the graph due to hydrocarbon-based bacteria as reported in a previous study of Frederick C. Neidhardt. The pattern of results resembled previous studies by K Yang et al., 2010 [62] and R A Naikoo et al., 2016 [63].

N-acetylcysteine is used to remove the biofilm developed around the steel bar which is further sonicated to homogenize in buffered peptone water used as a dilutant, 10x10^9 bacterial cell/ml following procedure reported in Ercole, C. et al., 2003 [64]. The thickness of biofilm is quantified by the volumetric changes by the liquid displacement method. Steel rebar was put in a cylinder filled with water up to a marked value. The value of volume recorded before and after the inserted rebar. The same procedure was then repeated for the same rebar with biofilm on it and the thickness of the rebar was calculated by following the formula given in equation (1).

$$A = Volume\ of\ Water, L = Marked\ length$$

$$B = Volume\ of\ Water + Steel\ bar\ submerged\ in\ water\ up - to\ marked\ length$$

$$C = Volume\ of\ Water + Steel\ bar\ submerged\ in\ water\ up - to\ marked\ length + Biofilm\ formed\ up - to\ marked\ length$$

$$Thickness\ of\ Biofilm = \frac{(C-B)}{((B-A)/L)} \tag{1}$$

Biofilm thickness of 0.02 mm,0.03 mm,0.025 mm, 0.03 mm,0.04 mm and 0.04 mm were reported for e. coli, e. coli with ZNMPs, bacillus subtilis, e. coli with INMPs, bacillus subtilis with ZNMPs and bacillus subtilis with INMPs respectively.

$$A = Weight\ of\ steel\ Bar\ before\ biofilm, L = Marked\ length$$

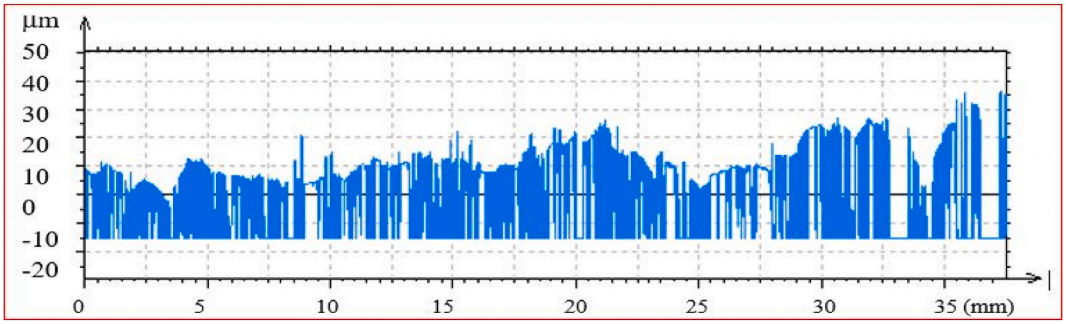

Fig. 8a. Profile of biofilm plotted by profilometer.

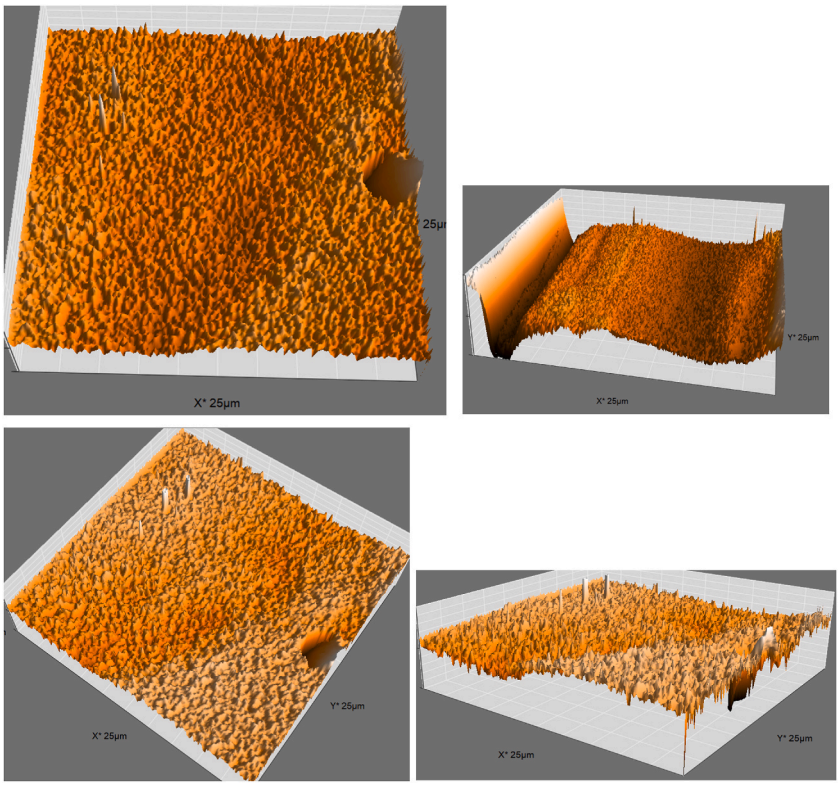

Fig. 8b. Profile of biofilm plotted by atomic force microscopy.

$$B = wt.\ of\ steel\ bar\ after\ biofilm\ formation\ (Normal\ dried)$$

$$Weight\ of\ Biofilm = (B - A),\ Weight\ of\ Biofilm\ /\ Length = (B - A)\ /L \quad (kg\ /\ ft)$$

$$Percentage\ weight\ gain = ((B - A)\ /\ A) \times 100 \tag{2}$$

Weight gain of biofilm of e. coli, e. coli with ZNMPs, bacillus subtilis, e. coli with INMPs, bacillus subtilis with ZNMPs and bacillus subtilis with INMPs were 2 %,3 %,4.67 %,4.8 %,5.92 % and 6 % respectively. Weight gain percentage was calculated by using equation (2). The physical changes in the steel rebars were carried screw gauge and by volumetric assessment 24 µm average increase in diameter was reported.

Surface profilometry was done by 2D Non-Contact Profilometer PS-50, NANOVEA to investigate the surface profile, roughness, and thickness of biofilm. For this purpose, the first film was formed on the surface of steel metal plates by dipping them in a bacterial solution of Bacillus s subtilis and *E. coli*. The surface profile developed by bacteria was rough and in micrometer variations. The average and maximum thickness of biofilm were reported as 12 and 38 µm respectively for the CMFB which is reported maximum among all six formulations. Results of profilometry are shown in Fig. 8 (a) taking the length of the specimen at the x-axis and biofilm thickness and

Table 6
Mix Design.

Material	CM0	CMB	CME	CMZB	CMZE	CMFB	CMFE
Cement $\left(Kg/m^3\right)$	257	257	257	257	257	257	257
F.A $\left(Kg/m^3\right)$	589	589	589	589	589	589	589
C.A $\left(Kg/m^3\right)$	643	643	643	643	643	643	643
BS (film on rebar)	–	Yes (amount)	–	yes	–	yes	–
EC (film on rebar)	–	–	yes	–	yes	–	yes
Calcium Lactate (g)	–	12	12	12	12	12	12
Fe_3O_4 (film on rebar)	–	–	–	–	–	yes	yes
Zeolite (film on rebar)	–	–	–	yes	yes	–	–
S.P $\left(L/m^3\right)$	0.8995	0.8995	0.8995	0.8995	0.8995	0.8995	0.8995

the y-axis. The results of roughness are close to those of V Gabe et al., 2019 studies [65].

(Length = 35 mm, Avg thickness = 12 μm, scale = 10 μm)

For the assessment of the surface texture and bonding of biofilm with the surface of pristine metal, the technique of atomic force microscopy (AFM) is used. A steel coupon with a biofilm layer of Bacillus subtilis and *Escherichia coli* developed on its surface was dried for 24 h in an incubator. Results of the AFM shown in Fig. 8 (b) depict that bacterial biofilm on the surface of steel was rough in texture and firmly bonded.

3.2. Design mix

The cement mix ratio for the specimen preparation was 1:2.2:2.4 for the cement, fine aggregate, and coarse aggregate respectively. The water-to-cement ratio was maintained at 0.4 for the hydration reactions of cement. Superplasticizer *"chemrite 303"* was used to attain good workability of concrete 100 mm × 200 mm sized plane and reinforced concrete cylindrical specimens were cast for this study. A total of seven formulations were planned, starting from control to the modified. The first was a control mix (CM0) without any treatment of steel bars. In the second formulation, an *e. coli* biofilm-coated steel bar was embedded at the center of cylinders (CME), the third was added with Bacillus subtilis biofilm (CMB), fourth was added with zeolite and e. coli biofilm (CMZE), the fifth was added with zeolite and bacillus subtilis biofilm (CMZB), sixth was added with iron oxide and e. coli biofilm (CMFE) and seventh was added with iron oxide and bacillus subtilis biofilm (CMFB) as shown in Table 6. Six plane concrete specimens were cast to check the target properties of the concrete mix.

The above-mentioned seven formulations were reinforced with a #3 steel bar placed at the center of the specimen and biofilm was developed on the surface of steel rebars by moving the bacterial solution 360^0 around the bars. Bacterial food was calcium lactate and put on the bar as the envelope of calcium lactate around the biofilm placing it in a measuring cylinder for 4 min. Concrete components were first dry mixed in a mixer and the wet mixing was done for 3–4 min and then placed in molds.

Molds of 100 mm × 200 mm were used, and the material was mixed in a mixer machine and then poured into molds and vibrated by a vibrator. After 24 h, specimens were unmolded and cured for 28 days at 100 % humidity at 23 ± 2^0C.

The compressive strength of plane concrete samples was studied by following ASTM C39 [66] procedure at a loading rate of 0.25 MPa/s. Cylindrical concrete samples of size 100 mm × 200 mm were tested after 28 days of curing. The cylinders were taken out of the curing tank and dried in air for 24 h before performing a compression test. In addition, the cylinder's top surface was smoothened by capping by "Plaster of Paris" to distribute the load equally on the top surface of the specimen. The average reported compressive strength was 31.63 MPa. Ultrasonic pulse velocity test was performed following ASTM C597 [67], where the time of transit (microseconds) of a vibrational pulse through plane concrete cylinders was checked for verification of mix quality. The average reading was 37 s, which was within the allowable limits.

The 28-day water-cured reinforced concrete samples were recurred in 5 % NaCl solution for 56 days to accelerate the corrosion samples. The test was performed on a multi-chem Gamery 750 test series to get anodic and cathodic polarization curves. The electrolyte was prepared with a 5 % NaCl solution in filtered water that provides a pathway for the migration of ions and electrons between both electrodes (cathode and anode). Copper and graphite were used as reference and counter electrodes, respectively.

Particle size and shape, elemental composition, and surface morphology of concrete samples were determined by Scanning Electron Microscopy (SEM) and Energy Dispersive X-ray (EDX) respectively. "*TESCAN VEGA3*" was used to perform SEM and EDX. Samples from the different portions of concrete specimens were removed carefully from ITZ of steel and concrete and calcite precipitation by the bacterial strains was studied by the SEM-EDX.

The compressive force was applied diametrically on cylindrical samples of reinforced concrete of size 100 mm × 200 mm along the length of the samples. The test was performed before and after the corrosion of samples. Arrangements for the test were made following ASTM C496 [68]. The tensile strength of the specimens was calculated by equation (3).

$$T = 2P \,/\, \pi LD \tag{3}$$

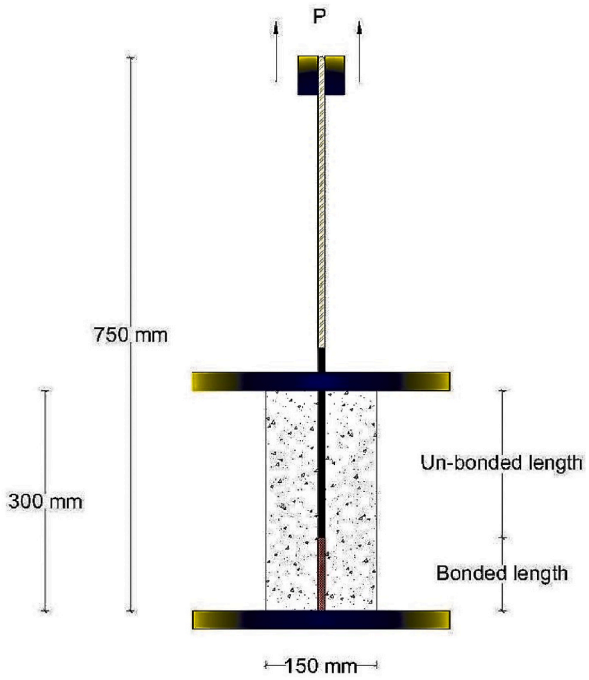

Fig. 9a. Pullout test arrangements.

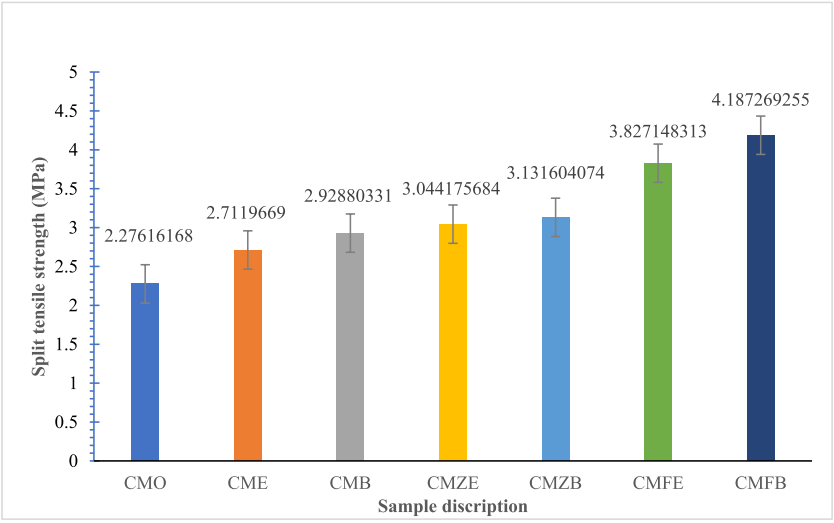

Fig. 9b. Results of split tensile strength.

where T is tensile Strength in MPa, P is the maximum applied load in Newtons, L is the length of specimens in mm, and D is the diameter of specimens in mm. A pullout test was performed to assess the bond strength of the steel-concrete interfacial zone. Concrete cylinders were added inside steel rebars at the center and a pull-out load was then applied. Steel rebars are bonded to some development length as shown in Fig. 9 (a).

The development length used for the test was 10 times the bar diameter. An assembly of two steel plates and four steel rods was used to hold the specimen and a pullout load was applied by a Universal testing machine (UTM) at the rate of 2.5 MPa/s. Bond strength is then calculated by equation (4).

$$B.S = P / \pi dl \tag{4}$$

X-ray diffraction tests on the concrete specimens were performed. The samples were selected from the concrete that stayed bound with steel rebar after splitting the specimen by split cylinder test. The powder samples were prepared and tested by K- α 1

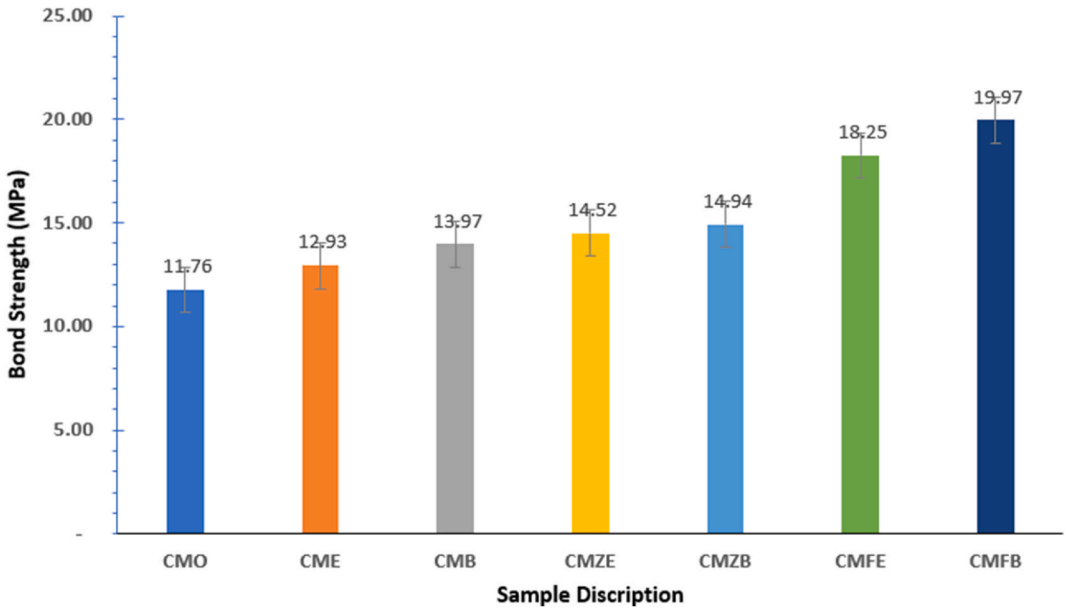

Fig. 9c. Results of bond strength.

diffractometer *"Burker D8 advanced"*. The angle range was selected from 10^{o} to 90^{o} with 2Θ feeding and high flux resolution.

Complexometric titration was performed on the specimens that were tested for X-ray diffraction to find out the percentage of calcium carbonates in the specimens. The test was performed following the ASTM D2613 testing procedure.

4. Results and discussion

4.1. Split cylinder test

It is concluded from the test that bacterial samples gave maximum strength due to good bond strength between concrete and steel. Specimens with bacterial strains hosted by carrier medium stayed almost unaffected by the corrosive environment. The results of split tensile strength are shown in Fig. 9 (b). The bacterial strains develop biofilm around the rebars, and the bond zone of concrete and steel is refined. A sticky layer of biofilm around the steel bars not only gives extra strength to the concrete steel bond but also enhances the immunity of the steel against corrosion. Literature pointed out that B. subtilis and *E. coli* are biofilm-forming bacteria. It is because of the metabolic activities of B. subtilis and *E. coli* which is the reason to produce biofilm products. Improvement in the split tensile strength of concrete by biological additions was reported by Gandhimathi et al., 2015 [69]. CMFB and CMFE specimens showed maximum tensile strength due to the highest concentration calcite deposit and proper packing and densification of the microstructure of concrete internally. Iron oxide and bacterial strains remain more compatible and form a thicker layer of biofilm that further activates more metabolic activities of bacteria and refines the internal structure of concrete.

CMZE and CMZB produced silicate products due to the presence of zeolite silicates and bacterial activity was also available by side. Samples without carrier media (CMB, CME) gave positive results but remained intermediate due to the lower survival rate of bacteria due to the harsh environment. Control samples remain consistent due to the corrosive environment provided to specimens to accelerate corrosion.

4.2. Pullout test

The results of bond strength are shown in Fig. 9 (c). The bacterial strains developed a sticky layer of biofilm around the steel bars giving extra strength to the concrete steel bond. The metabolic activities of *B. subtilis* and *E. coli* produced biofilm products. Maximum bond strength was shown by the CMFB followed by CMFE specimens because of its denser microstructure by calcite deposition of the microbial layers. Iron oxide and zeolite being carrier medium for the bacterial strains made the environment compatible for biofilm durability. The bond strength of the reinforced concrete was improved by 69.8 % when *B.subtilis* was incorporated with iron oxide followed by *E.coli* with iron oxide resulting in 5a 5.2 % improvement in bond strength.

4.3. Scanning Electron Microscopy (SEM) and Energy Dispersive X-ray spectroscopy

SEM micrographs were taken on different resolutions and magnifications and EDX results confirmed the formation of calcite. The presence of calcite was confirmed by comparing the structure with already present literature. Nano and micro-size images taken by

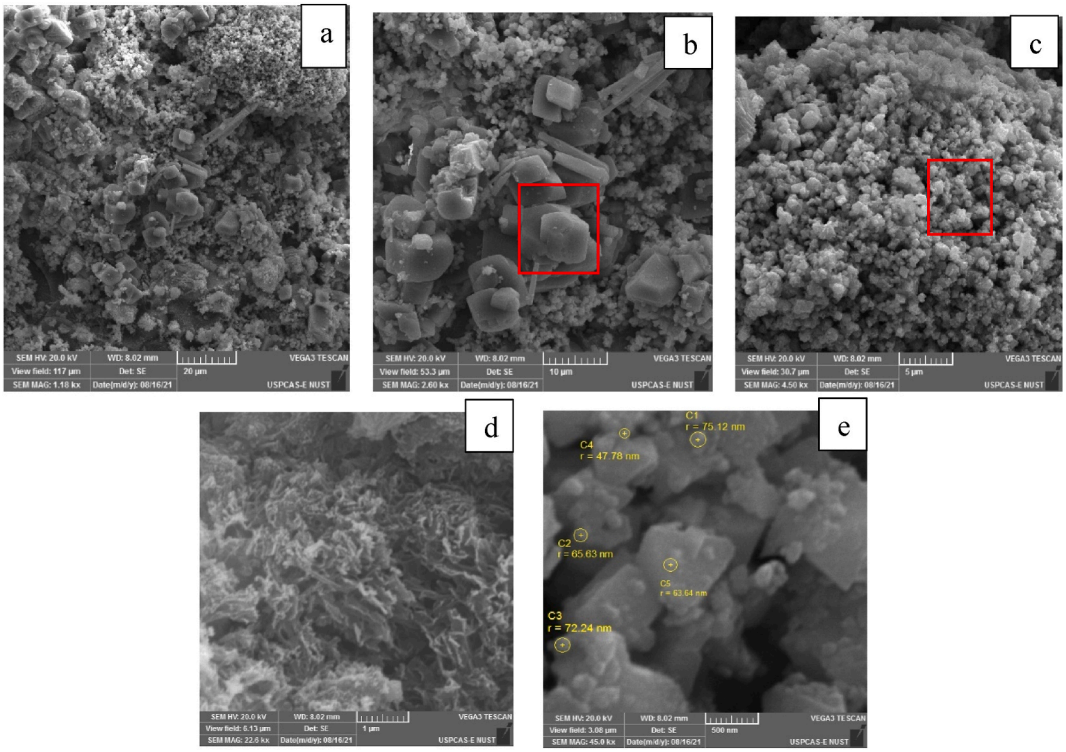

Fig. 10. (a) Concrete microstructure SEM Image (b) Calcite crystals rhombohedral (c)Nano-micro particles in concrete structure (d) Microbiologically deposited calcite (e) Nano-level view of calcite crystal.

SEM matched with R. Saddique et al., 2011. Further confirmation of the calcite and silicates was done by EDX which reported the presence of calcium, oxygen, carbon, silicon, and other additives the percentages of elements are given in EDX resultant tables, and their compositions showed a resemblance with construction building materials, 25 (2011) [70].

Elements like carbon, oxygen, and calcium confirm calcite, and calcium, silicon, and oxygen confirm the presence of calcium silicate due to the presence of bacterial media and zeolite carrier media. Iron was present due to iron oxide being used as a carrier medium. Microstructure refinement of concrete structure is clear from SEM images shown in Fig. 10 (a) and 10 (c), calcite crystals are shown in Fig. 10 (b) and details of bacterial deposits can be seen in Fig. 10 (d) and 10 (e). A concrete chunk scratched from a steel bar shows clear precipitation of calcite on its surface shown in Fig. 11 (a), (b), and (c). Needle-like products on the specimen taken from the interfacial zone were captured, as shown in Fig. 11 (d) and 11 (e).

EDX results of concrete specimens showed a good percentage of calcium and elements like oxygen, carbon led to the final chemistry of the product which is $CaCO_3$ shown in Fig. 12 (a) and spectrum 1 and nano deposits have iron and silica-based deposits as well that highlight concrete microstructure refinement by the nano media and the percentage composition is shown in Fig. 12 (b) and spectrum 2.

Above mention SEM micrographs give the needle-like structure of ettringite and plates of calcite in all bacterial samples including CME, CMB, CMZE, CMZB, CMFE, and CMFB. CMFB showed the most refined internal microstructure. The refinement and calcite production order in specimens is

$$CMO < CME < CMB < CMZE < CMZB < CMFE < CMFB$$

EDX results represented that calcite produced by the specimens having iron oxide in them had more percentages of calcium carbonate and specimens which were having zeolite as carrier medium had a percentage of calcium silicate. Specimens with bacteria had calcite and the least amount of calcium carbonate was reported in CMO samples.

4.4. X-ray diffraction (XRD)

The test was performed to check elemental composition, nature of structure (crystalline or amorphous), micro-strained, and dislocation densities with authenticity. All the peaks of diffraction were identified by the expert high scope and the peaks were labeled accordingly. Calcite is the most intensive peak for all the above plots which support the SEM and EDX results. The availability of silicate in zeolite-containing specimens and the presence of iron in iron oxide-containing specimens is also confirmed and the availability of carbon is due to the availability of bacterial cells. Peaks of calcite and quartz were reported in XRD graphs which were closely matched with the JCPDs 5–586 [71] shown in Fig. 13(a)–(g). High-intensity calcite products is reported for the CMFB and CMZB.

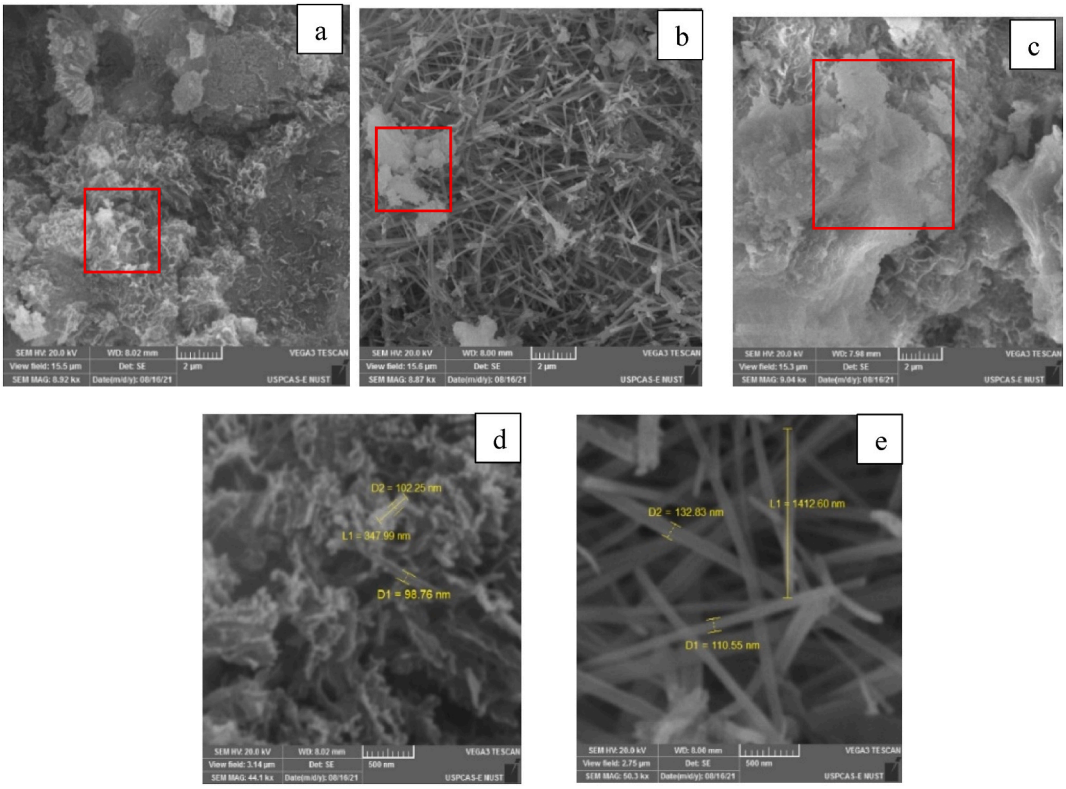

Fig. 11. (a) SEM Images of calcite deposited by microbes (b) SEM Images of microbial products (c) SEM Images of calcite crystals (d) Microstructure refinements images at nano level (e) Bacterial rod shape deposits around steel surface.

CMFE and CMZE remained the second intensive formulation and then intensity decreased from CMB, CME, and CM0 specimens, respectively. The order of intensities is given below.

$$CMO < CME < CMB < CMZE < CMFE < CMZB < CMFB$$

4.5. Complexometric Titration

Specimens were scraped out from the interfacial zone and then ground to powder, and the suspension was formed with distilled water and put in the rotatory drive for 24 h. EDTA, buffer solution with pH 10 range, and Eriochrome black T were used as titrant and indicator, respectively the arrangement for the test is shown in Fig. 14 following the standard procedure reported by M. Cecilia Yappert et al., 1997 [72]. Complexometric titration for finding the percentage of calcium carbonate is reported in the results of calcium carbonate percentage was reported maximum for CMFB sample which 31.3 % and were 29.6 %, 24.7 %, 22.8 %, 20.1 %, 20.4 % and 17.9 % for CMFE, CMZB, CMZE, CMB, CME and CMO respectively. The calculation for the percentage of calcium carbonate in concrete powder was done by following formulae.

$$Percentage\ of\ calcium\ carbonate = \frac{Quantity\ of\ Calcium\ by\ Titration}{Weight\ of\ Powder\ Mixed} \times 100$$

$$mg\ of\ calcium\ carbonate = \frac{A \times B}{ml\ of\ Sample}$$

where,

$A = ml\ of\ EDTA\ used\ for\ sample - ml\ of\ EDTA\ used\ blank$

$B = mg\ of\ CaCO_3\ equivalent\ to\ 1\ ml\ EDTA\ titrant$

4.6. Tafel polarization

Specimens after curing in the corrosive environment for 56 days were tested for corrosion. Tafel plots were obtained as output in

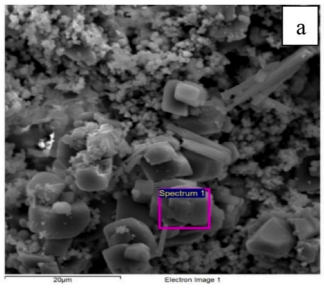

Element	Weight%	Atomic%
C	13.97	22.29
O	50.97	61.06
Si	0.61	0.42
Ca	32.63	15.60
Fe	1.82	0.62
Totals	100.00	

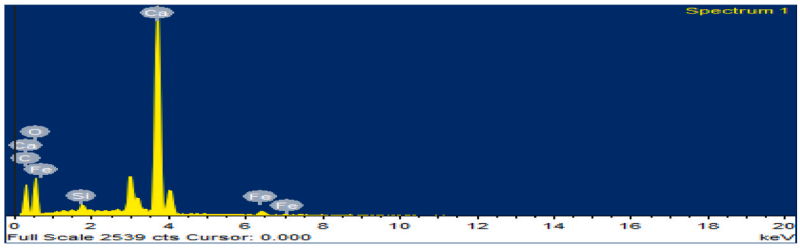

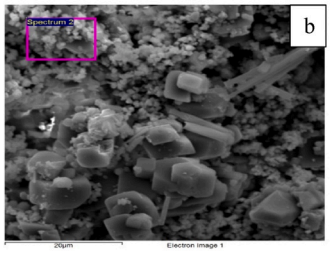

Element	Weight%	Atomic%
C	12.19	20.39
O	48.97	61.49
Ca	29.30	14.69
Fe	9.54	3.43
Totals	100.00	

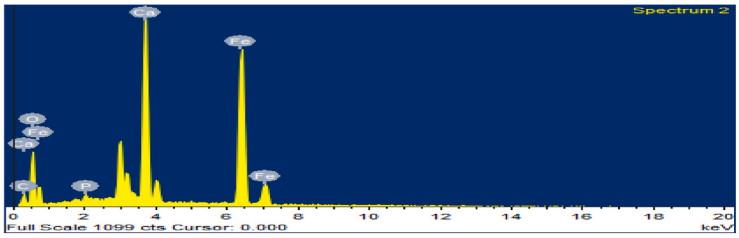

Fig. 12. (a) EDX results of concrete specimen (b) EDX results of nano deposits.

which current density and polarization voltage were piloted on the x and y axis respectively as shown in Fig. 15. The resultant perimeters were obtained from the cathodic and anodic curves like corrosion rate (CR), corrosion resistance (R_p), and corrosion inhibition efficiency (η). Equations (5) and (6) are used for the calculations.

$$Rp\ (\Omega) = \frac{\beta_a X\ \beta_c}{(\beta_a + \beta_c) X\ 2.303 X\ i_{corr}} \tag{5}$$

$$\eta\ (\%) = \frac{i_{corr}(\mathrm{CM}) - i_{corr}}{i_{corr}\ (CM)}\ X100 \tag{6}$$

The values of anodic and cathodic Tafel slopes were found by fitting the Tafel plots on the origin pro by placing a horizontal line a trisection point was selected and I_{corr} and slopes values were determined. Results of the corrosion rate (CR), corrosion resistance (R_p), and corrosion inhibition efficiency (η) are listed in Table 7.

Results declared that the CMFB formulation was the most efficient and showed 78.5 % corrosion inhibition and showed maximum polarization resistance of 1478.6 Ω. CMFE formulation was the second-best formulation and provided 72.7 % corrosion inhibition and showed 1298.42 Ohm polarization resistance. Bacteria with zeolite provided more efficient results than the plan bacterial formulations and their results were 61.3 %, 56.8 %, 31.2 %, and 29.4 % corrosion inhibition for CMZB, CMZE, CMB, and CME respectively. The polarization resistance values were 1020.5, 909.85, 591.4, and 494.1 Ohms for CMZB, CMZE, CMB, and CME respectively. Maximum 60 % corrosion inhibition efficiency reported in studies Ali A. et al., 2017 [73] which showed that this study has acceptable results.

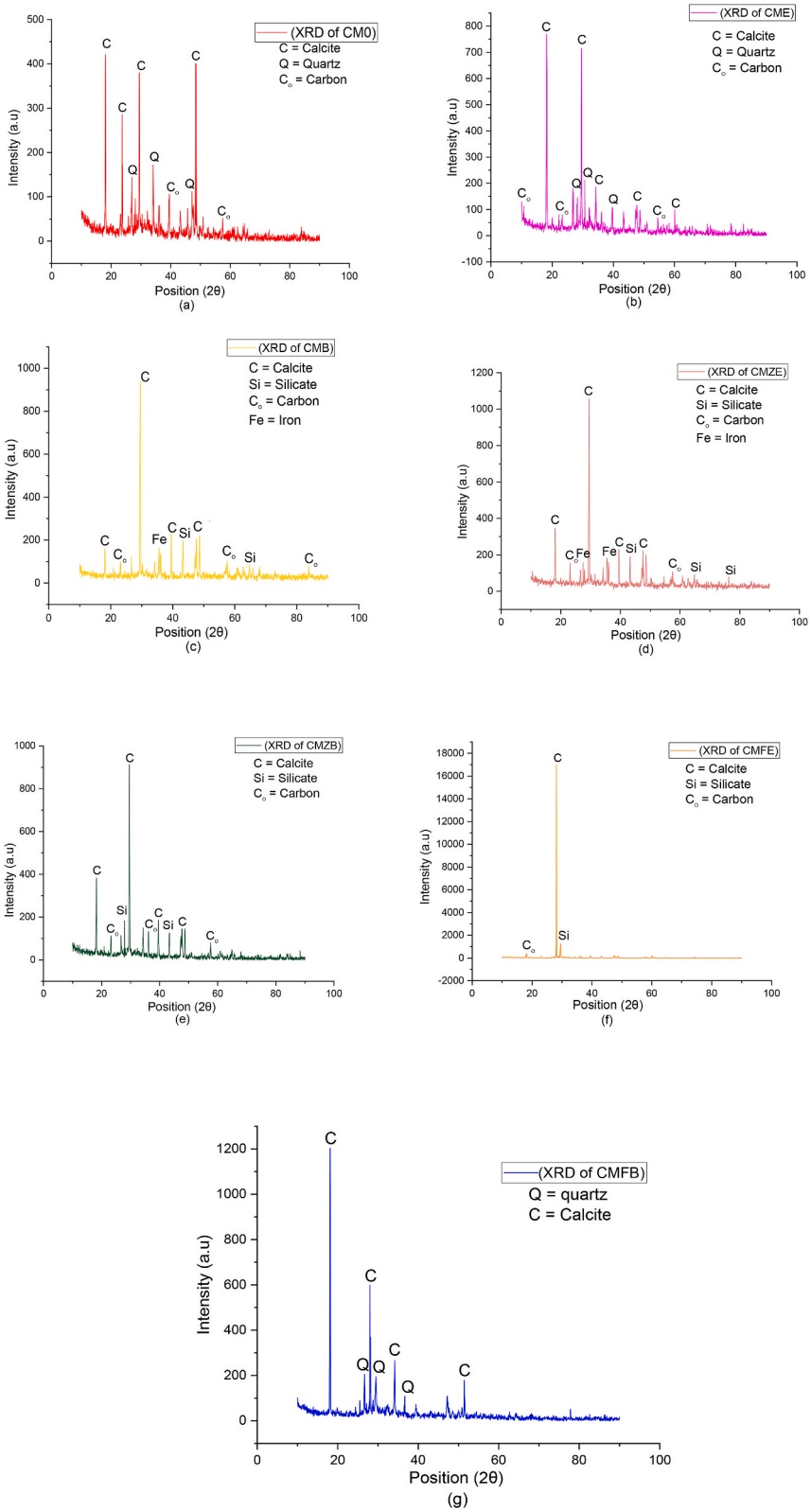

Fig. 13. XRD results of (a) Control mix (b) *E. coli* biofilm-coated steel bar (c) Bacillus subtilis biofilm-coated steel bar (d) Zeolite plus e. coli biofilm (e) Zeolite and bacillus subtilis (f) Iron oxide and e. coli (g) Iron oxide and bacillus subtilis.

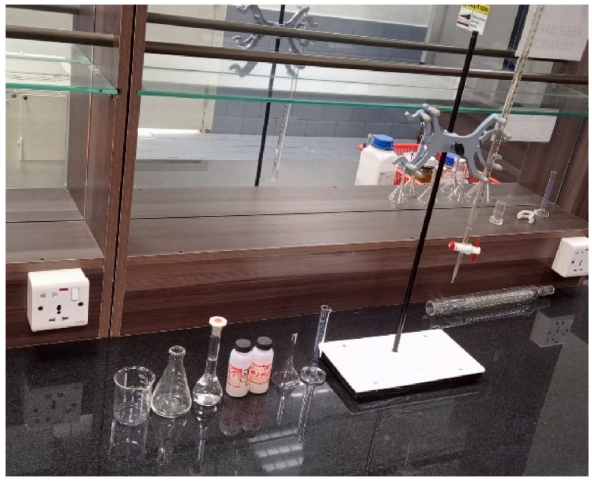

Fig. 14. Arrangement for complexometric titration.

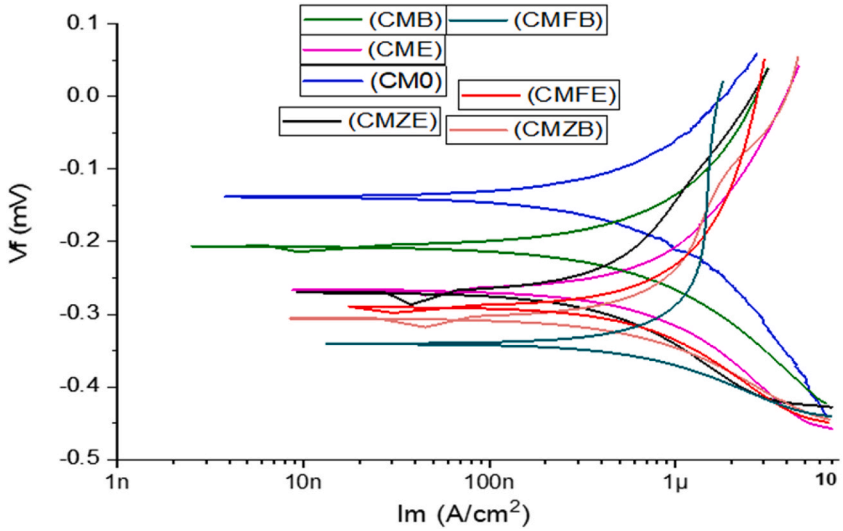

Fig. 15. Tafel polarization anodic and cathodic slopes calculations.

Table 7
Results of Tafel polarization perimeters.

Sample ID	E_{corr} (mV)	I_{corr} (µA)	β_α x e $^{-3}$ (V/decayed)	βc x e $^{-3}$ (V/decayed)	CR x e $^{-3}$ (mpy)	$R_{p\ max}$ (Ω)	η (%)
CM0	−483	68.20	387.4	223.9	495.2	386.7	0
CME	−326.5	53.80	337.9	210.6	402.5	494.1	29.4
CMB	−236	44.9	307.6	198.8	296.7	591.4	31.2
CMZE	−198.5	42.3	331.4	298.5	189.5	909.85	56.8
CMZB	−178.4	35.8	375.4	296.7	176.8	1020.5	61.3
CMFE	−156.2	55.3	272.5	217.4	153.4	1298.42	72.7
CMFB	−49.7	40.20	254.7	245.3	117.2	1478.6	78.5

4.7. R_p/E_C test

According to the resultant plot polarization resistance of CMFB composition was 998 Ω which was the maximum among all formulations. CMFE showed 920.7 Ω polarization resistance, and other formulations like CMZB, CMZE, CMB, CME, and CM0 showed 854.2 Ω, 747.6 Ω, 458.3 Ω, 362.7 Ω and 347.8 Ω polarization resistance respectively as shown in Fig. 16 (a).

According to the resultant plot of corrosion rate of CMFB composition was 9.3 (mpy) which was the minimum among all

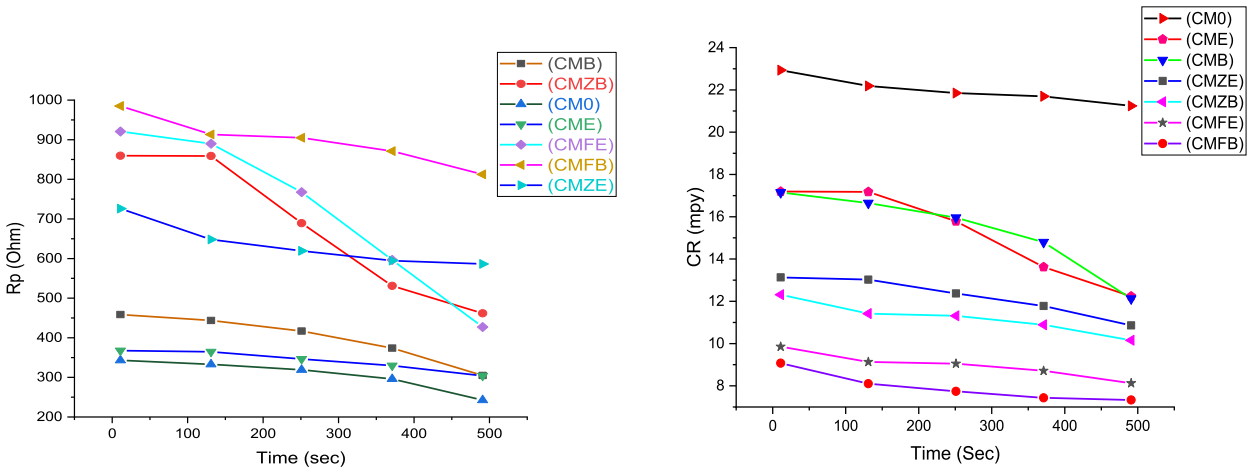

Fig. 16. (a) Results of polarization resistance (b) Results of corrosion rate.

formulations. CMFE showed 9.9 (mpy) corrosion rate, and other formulations like CMZB, CMZE, CMB, CME, and CM0 showed 12.7 (mpy), 13.2 (mpy), 15.1(mpy), 15.1(mpy), and 23.4 (mpy) corrosion rate respectively as shown in Fig. 12 (b). A corrosion rate of 16.3 (mpy) was reported by Ghafari et al., 2013.

5. Conclusion

It is concluded from this study that concrete microstructure refinement and biofilm around the steel bar led to the following results:

- Biofilm with an average thickness of 12 μm was successfully developed on steel rebar to act as the passive protective layer against corrosion for *bacillus subtilis* with iron oxide, least biofilm was developed by the *e.coli* without any carrier medium which was 7 μm on average which is more than *P. aeruginosa* resulted in 6 μm biofilm development previously by SV Oopath et al., 2022.
- Biologically encapsulated steel-embedded concrete provided 78.5 % corrosion inhibition efficiency and 998 Ω polarization resistance which is 159 % more than the control. The corrosion rate was reduced by 60.25 % due to the protective biofilm layer and refinement of the concrete microstructure *e.coli* without carrier medium showed the least corrosion resistance of 29.4 % owing to the thin protective layer.
- Split tensile strength was successfully improved by 84.2 % due to the roughness of biofilm and bacteria calcite precipitation in the interfacial bond zone, *e.coli* without carrier medium resulted in the least improvement of 19.4 %.
- Bond strength of steel-embedded concrete specimens was enhanced by 59.8 % at maximum when *bacillus subtilis* with iron oxide was used as a protective layer around steel rebars, followed by the *E.coli* with iron oxide showed a 55.2 % improvement in bond strength than the control mix.

6. Limitation and recommendation

This study is limited to normal bacterial strains which are not strained in any chemical environment. It is recommended that genetic modification and biologically trained bacteria be incorporated into concrete to obtain targeted properties of concrete. Biochemical mimicry can also be implemented to attain good results.

Data availability

Data will be made available on request.

CRediT authorship contribution statement

Sajid Rasheed: Formal analysis, Data curation, Conceptualization. **Rao Arslan Khushnood:** Supervision. **Ali Raza:** Writing – review & editing, Writing – original draft, Visualization, Validation, Supervision, Software, Resources, Project administration, Methodology, Investigation, Funding acquisition, Formal analysis, Data curation, Conceptualization. **Sajjad Ahmed:** Project administration. **Maria Kanwal:** Software.

Declaration of competing interest

The authors declare the following financial interests/personal relationships which may be considered as potential competing interests:Sajid Rasheed reports article publishing charges was provided by National University of Science and Technology. If there are other authors, they declare that they have no known competing financial interests or personal relationships that could have appeared to influence the work reported in this paper.

Appendix A. Supplementary data

Supplementary data to this article can be found online at https://doi.org/10.1016/j.heliyon.2024.e37966.

References

[1] K. van Breugel, Is there a market for self-healing cement-based materials?. First International Conference on Self Healing Materials, 2007, pp. 1–9.
[2] N. Roghanian, N. Banthia, Development of a sustainable coating and repair material to prevent bio-corrosion in concrete sewer and waste-water pipes, Cem. Concr. Compos. 100 (2019) 99–107, https://doi.org/10.1016/J.CEMCONCOMP.2019.03.026.
[3] C. Meyer, Concrete materials and sustainable development in the United States, 83, Concrete Materials and Sustainable Development (1992) 1–10.
[4] Z.S. Maria Kanwala, Robabeh Bagheri, Abdul Ghafar Wattoo, Muhammad Imran Irshad, Rao Arsalan Khushnood, Biological corrosion inhibitors for concrete, in: M.L. Inamuddin, Mohd Imran Ahamed, Rajender Boddula (Eds.), Theory and Applications of Green Corrosion Inhibitors, 86th ed., Materials Research Foundations, 2021, pp. 183–203, https://doi.org/10.21741/9781644901052-7.
[5] W. Wang, C. Lu, Time-varying law of rebar corrosion rate in fly ash concrete, J. Hazard Mater. 360 (2018) 520–528, https://doi.org/10.1016/j.jhazmat.2018.08.007.
[6] Y. Wang, Y. Zuo, Y. Tang, Inhibition effect and mechanism of sodium oleate on passivation and pitting corrosion of steel in simulated concrete pore solution, Constr Build Mater 167 (2018) 197–204, https://doi.org/10.1016/J.CONBUILDMAT.2018.01.170.
[7] J.K. Das, B. Pradhan, Effect of cation type of chloride salts on corrosion behaviour of steel in concrete powder electrolyte solution in the presence of corrosion inhibitors, Constr Build Mater 208 (2019) 175–191, https://doi.org/10.1016/J.CONBUILDMAT.2019.02.153.
[8] T. Kiran, D. Andrushia, C. El Hachem, B. Kanagaraj, A. N, M. Azab, Effect of nano cementitious composites on corrosion resistance and residual bond strength of concrete, Results in Engineering 18 (2023), https://doi.org/10.1016/j.rineng.2023.101064.
[9] S. Anand Kumar, G. Sudheer, Influence of the oxide layer on the quality of bonding in adhesively bonded metallic structures by ultrasonic guided waves, Int. J. Adhesion Adhes. 111 (2021), https://doi.org/10.1016/j.ijadhadh.2021.102981.
[10] T. Kiran, N. Anand, S. Nitish Kumar, D. Andrushia, S.K. Singh, P. Arulraj, Influence of nano-cementitious materials on improving the corrosion resistance and microstructure characteristics of concrete, J. Adhes. Sci. Technol. 35 (2021), https://doi.org/10.1080/01694243.2020.1870083.
[11] V.H. Dang, R. François, Influence of long-term corrosion in chloride environment on mechanical behaviour of RC beam, Eng. Struct. 48 (2013) 558–568, https://doi.org/10.1016/j.engstruct.2012.09.021.
[12] A.A. Almusallam, Effect of degree of corrosion on the properties of reinforcing steel bars, Constr Build Mater 15 (2001) 361–368, https://doi.org/10.1016/S0950-0618(01)00009-5.
[13] K. Sadeghi, M.K. Musa, H.M. Nassrullah, Corrosion problems in RC structures : an overview of causes , mechanism, effects, controls and evaluation, Acad. Res. Int. 10 (2019) 15–28.
[14] A.A. Almusallam, Effect of degree of corrosion on the properties of reinforcing steel bars, Constr Build Mater 15 (2001) 361–368, https://doi.org/10.1016/S0950-0618(01)00009-5.
[15] A. Imam, S. Mishra, Y.K. Bind, Review study towards corrosion mechanism and its impact on the durability of concrete structures, AIMS Mater Sci 5 (2018) 276–300, https://doi.org/10.3934/matersci.2018.2.276.
[16] Highway Maintenance Market Report - UK 2019-2023 - AMA Research, (n.d.). https://www.amaresearch.co.uk/report/highway-maintenance-market-report-uk-2019-2023/(accessed November 2, 2023).
[17] J. Bilcik, I. Holly, Effect of reinforcement corrosion on bond behaviour, Procedia Eng. 65 (2013) 248–253, https://doi.org/10.1016/j.proeng.2013.09.038.
[18] K. Andisheh, A. Scott, A. Palermo, Seismic behavior of corroded RC bridges: review and research gaps, International Journal of Corrosion 2016 (2016), https://doi.org/10.1155/2016/3075184.
[19] A. Raza, R.A. Khushnood, Repair of mortar cracks using Bacillus pumilus based bio-suspension assessed by machine learning algorithm for image processing, J. Build. Eng. 61 (2022) 105267, https://doi.org/10.1016/J.JOBE.2022.105267.
[20] B.A.R. Chini, S.F. Bruening, REPORT 10 DECONSTRUCTION AND MATERIALS REUSE IN THE UNITED, (n.d.).
[21] A. Raza, R.A. Khushnood, Bacterial carbonate precipitation using active metabolic pathway to repair mortar cracks, Materials 15 (2022) 6616, https://doi.org/10.3390/MA15196616/S1.
[22] W. Virginia, Study of Reinforced Concrete Building Demolition Methods and Code Requirements Study of Reinforced Concrete Building Demolition Methods and Code Requirements by A Thesis Is Submitted to the at West Virginia University for the Degree of Master of Science I, 2007.
[23] T.K. Kim, S.J. Choi, J.H.J. Kim, Y.S. Chu, E. Yu, Performance based evaluation of carbonation resistance of concrete according to various curing conditions from climate change effect, Int J Concr Struct Mater 11 (2017) 687–700, https://doi.org/10.1007/s40069-017-0206-7.
[24] EonCoat - a Fundamentally Different Coating Technology, (n.d.).
[25] J.P. Broomfield, Physical and chemical repair and rehabilitation techniques, Corrosion of Steel in Concrete (2010) 112–139, https://doi.org/10.4324/9780203414606_chapter_6.
[26] H. Saricimen, K. Attar, M. Maslehuddin, I. Asfaha, M. Shameem, M.S. Barry, Blistering of Epoxy Coating on Concrete Floor, (n.d.) 288–297.
[27] T.R. Wilkinson, Survival of bacteria on metal surfaces, Appl. Microbiol. 14 (1966) 303–307, https://doi.org/10.1128/aem.14.3.303-307.1966.
[28] H. Liu, T. Gu, Y. Lv, M. Asif, F. Xiong, G. Zhang, H. Liu, Corrosion inhibition and anti-bacterial efficacy of benzalkonium chloride in artificial CO2-saturated oilfield produced water, Corros Sci 117 (2017) 24–34, https://doi.org/10.1016/j.corsci.2017.01.006.
[29] H.P. Volkland, H. Harms, K. Knopf, O. Wanner, A.J.B. Zehnder, Corrosion inhibition of mild steel by bacteria, Biofouling 15 (2000) 287–297, https://doi.org/10.1080/08927010009386319.
[30] H.Z. Wadood, A. Rajasekar, Y.P. Ting, A.N. Sabari, Role of Bacillus subtilis and Pseudomonas aeruginosa on corrosion behaviour of stainless steel, Arabian J. Sci. Eng. 40 (2015) 1825–1836, https://doi.org/10.1007/s13369-015-1590-4.
[31] J. Wu, D. Zhang, P. Wang, Y. Cheng, S. Sun, Y. Sun, S. Chen, The influence of Desulfovibrio sp. and Pseudoalteromonas sp. on the corrosion of Q235 carbon steel in natural seawater, Corros Sci 112 (2016) 552–562, https://doi.org/10.1016/J.CORSCI.2016.04.047.
[32] R. Mansour, A. Elshafei, Role of microorganisms in corrosion induction and prevention, Br. Biotechnol. J. 14 (2016) 1–11, https://doi.org/10.9734/bbj/2016/27049.
[33] M. Imran, A. Raza, M. Touqeer, Prediction of compressive strength of high-performance concrete (HPC) using machine learning algorithms, Multiscale and Multidisciplinary Modeling, Experiments and Design (2023) 1–14, https://doi.org/10.1007/S41939-023-00310-5/TABLES/3.

[34] A. Raza, R. Arsalan Khushnood, Digital image processing for precise evaluation of concrete crack repair using bio-inspired strategies, Constr Build Mater 350 (2022) 128863, https://doi.org/10.1016/J.CONBUILDMAT.2022.128863.
[35] N. Shaheen, R.A. Khushnood, W. Khaliq, H. Murtaza, R. Iqbal, M.H. Khan, Synthesis and characterization of bio-immobilized nano/micro inert and reactive additives for feasibility investigation in self-healing concrete, Constr Build Mater 226 (2019) 492–506, https://doi.org/10.1016/j.conbuildmat.2019.07.202.
[36] R.A. Khushnood, Z.A. Qureshi, N. Shaheen, S. Ali, Bio-mineralized self-healing recycled aggregate concrete for sustainable infrastructure, Sci. Total Environ. (2019) 135007, https://doi.org/10.1016/j.scitotenv.2019.135007.
[37] A. Ortega-Villamagua, E, M. Gudiño-Gomezjurado, Palma-Cando, Microbiologically induced carbonate precipitation in heritage materials, Molecules 25 (2020) 5499.
[38] Y. Su, J. Feng, P. Jin, C. Qian, Influence of bacterial self-healing agent on early age performance of cement-based materials, Constr Build Mater 218 (2019) 224–234, https://doi.org/10.1016/j.conbuildmat.2019.05.077.
[39] N. Chahal, A. Rajor, R. Siddique, Calcium carbonate precipitation by different bacterial strains, Afr. J. Biotechnol. 10 (2011) 8359–8372, https://doi.org/10.5897/ajb11.345.
[40] G.A. Silva-Castro, I. Uad, A. Gonzalez-Martinez, A. Rivadeneyra, J. Gonzalez-Lopez, M.A. Rivadeneyra, Bioprecipitation of calcium carbonate crystals by bacteria isolated from saline environments grown in culture media amended with seawater and real brine, BioMed Res. Int. 2015 (2015), https://doi.org/10.1155/2015/816102.
[41] A. Raza, R. Arsalan Khushnood, Digital image processing for precise evaluation of concrete crack repair using bio-inspired strategies, Constr Build Mater 350 (2022) 128863, https://doi.org/10.1016/J.CONBUILDMAT.2022.128863.
[42] M. Seifan, A.K. Sarmah, A.K. Samani, A. Ebrahiminezhad, Y. Ghasemi, A. Berenjian, Mechanical properties of bio self-healing concrete containing immobilized bacteria with iron oxide nanoparticles, Applied Microbiology and Biotechnology 2018 102 (10 102) (2018) 4489–4498, https://doi.org/10.1007/S00253-018-8913-9.
[43] M. Wu, X. Hu, Q. Zhang, D. Xue, Y. Zhao, Growth environment optimization for inducing bacterial mineralization and its application in concrete healing, Constr Build Mater 209 (2019) 631–643, https://doi.org/10.1016/j.conbuildmat.2019.03.181.
[44] S. Han, E.K. Choi, W. Park, C. Yi, N. Chung, Effectiveness of expanded clay as a bacteria carrier for self-healing concrete, Appl Biol Chem 62 (2019), https://doi.org/10.1186/s13765-019-0426-4, 0–4.
[45] R.V. Jasra, B. Tyagi, Y.M. Badheka, V.N. Choudary, T.S.G. Bhat, Effect of clay binder on sorption and catalytic properties of zeolite pellets, Ind. Eng. Chem. Res. 42 (2003) 3263–3272, https://doi.org/10.1021/ie010953l.
[46] C. Rodriguez-Navarro, F. Jroundi, M. Schiro, E. Ruiz-Agudo, M.T. González-Muñoz, Influence of substrate mineralogy on bacterial mineralization of calcium carbonate: implications for stone conservation, Appl. Environ. Microbiol. 78 (2012) 4017–4029, https://doi.org/10.1128/AEM.07044-11.
[47] ASTM, Astm C150, Standard Specification for Portland Cement, 2020.
[48] ASTM C 1018.Pdf, (n.d.).
[49] ASTM C 1018.Pdf, (n.d.).
[50] Astm C-33, Concrete 187 (2002) 25411.
[51] Astm C128, (n.d.) 5–8.
[52] American Society for Testing Materials, Astm C127, Standard Test Method for Density, Relative Density (Specific Gravity) and Absorption of Coarse Aggregate Philadephi, 2012.
[53] ASTM International, Astm A615, Astm A615, 2016, pp. 1–8.
[54] ASTM E572, (n.d.).
[55] ASTM A894, (n.d.).
[56] F. Zameer, J. Kreft, S. Gopal, Interaction of Listeria Monocytogenes and Staphylococcus Epidermidis in dual species biofilms, J. Food Saf. 30 (2010) 954–968, https://doi.org/10.1111/J.1745-4565.2010.00254.X.
[57] F. Zameer, S. Gopal, G. Krohne, J. Kreft, Development of a biofilm model for Listeria monocytogenes EGD-e, World J. Microbiol. Biotechnol. 26 (2010) 1143–1147, https://doi.org/10.1007/S11274-009-0271-4/FIGURES/3.
[58] F. Zameer, Impact of hydrogen peroxide on growth and survival of Listeria monocytogenes biofilms, Downloads.Hindawi.ComF Zameer, S GopalE-Journal of Chemistry, 2010•downloads.Hindawi.Com (n.d.), S.G.-E.-J. of Chemistry, undefined (2010). https://downloads.hindawi.com/journals/chem/2010/641563.pdf. (Accessed 2 November 2023).
[59] F. Zameer, J. Kreft, S. Gopal, Interaction of LISTERIA monocytogenes and STAPHYLOCOCCUS epidermidis in dual species biofilms, J. Food Saf. 30 (2010) 954–968, https://doi.org/10.1111/J.1745-4565.2010.00254.X.
[60] H. Afifudin, W. Nadzarah, M.S. Hamidah, H. Noor Hana, Microbial participation in the formation of calcium silicate hydrated (CSH) from Bacillus Subtilis, Procedia Eng. 20 (2011) 159–165, https://doi.org/10.1016/j.proeng.2011.11.151.
[61] K. Deplanche, I. Caldelari, I.P. Mikheenko, F. Sargent, L.E. Macaskie, Involvement of hydrogenases in the formation of highly catalytic Pd(0) nanoparticles by bioreduction of Pd(II) using Escherichia coli mutant strains, Microbiology (N. Y.) 156 (2010) 2630–2640, https://doi.org/10.1099/mic.0.036681-0.
[62] K. Yang, B. Xing, Adsorption of organic compounds by carbon nanomaterials in aqueous phase: polanyi theory and its application, Chem Rev 110 (2010) 5989–6008, https://doi.org/10.1021/cr100059s.
[63] R.A. Naikoo, S.U. Bhat, M.A. Mir, R. Tomar, W.A. Khanday, P. Dipak, D.C. Tiwari, Polypyrrole and its composites with various cation exchanged forms of zeolite X and their role in sensitive detection of carbon monoxide, RSC Adv. 6 (2016) 99202–99210, https://doi.org/10.1039/c6ra19708f.
[64] C. Ercole, M. Del Gallo, L. Mosiello, S. Baccella, A. Lepidi, Escherichia coli detection in vegetable food by a potentiometric biosensor, Sens Actuators B Chem 91 (2003) 163–168, https://doi.org/10.1016/S0925-4005(03)00083-2.
[65] C.A. Hage, E.M. Carmona, O. Epelbaum, S.E. Evans, L.M. Gabe, Q. Haydour, K.S. Knox, J.K. Kolls, M.H. Murad, N.L. Wengenack, A.H. Limper, Microbiological laboratory testing in the diagnosis of fungal infections in pulmonary and critical care practice: an official American thoracic society clinical practice guideline, Am. J. Respir. Crit. Care Med. 200 (2019) 535–550, https://doi.org/10.1164/rccm.201906-1185ST.
[66] ASTMC39, Astm C-39, Standard Test Method for Compressive Strength of Cylindrical Concrete Specimens, 2014.
[67] American Society for Testing and Materials, Astm C597, (2016) 1-4.
[68] ASTM, Astm C496, 2012, pp. 9–13.
[69] C. Gandhimathi, J.R. Venugopal, A.Y. Tham, S. Ramakrishna, S.D. Kumar, Biomimetic hybrid nanofibrous substrates for mesenchymal stem cells differentiation into osteogenic cells, Mater. Sci. Eng. C 49 (2015) 776–785, https://doi.org/10.1016/j.msec.2015.01.075.
[70] F. Pacheco-Torgal, S. Jalali, Nanotechnology: advantages and drawbacks in the field of construction and building materials, Constr Build Mater 25 (2011) 582–590, https://doi.org/10.1016/j.conbuildmat.2010.07.009.
[71] Study of the Photoluminescent Properties of Polyurethane-CaCO3 Composites for Bioapplications, (n.d.).
[72] M. Cecilia Yappert, Donald B. DuPre, Complexometric titrations: competition of complexing agents in the determination of water hardness with EDTA, J Chem Educ 74 (1997) 1422–1423.
[73] A.A. Abd-Elaal, N.M. Elbasiony, S.M. Shaban, E.G. Zaki, Studying the corrosion inhibition of some prepared nonionic surfactants based on 3-(4-hydroxyphenyl) propanoic acid and estimating the influence of silver nanoparticles on the surface parameters, J. Mol. Liq. 249 (2018) 304–317, https://doi.org/10.1016/j.molliq.2017.11.052.